Biogeochemical controls on the relative importance of denitrification and dissimilatory nitrate reduction to ammonium in estuaries

Adam J Kessler[1,2,*], Keryn L Roberts[2], Andrew Bissett[3], Perran L M Cook[2]

[1] School of Earth, Atmosphere & Environment, Monash University, Australia, 3800

[2] Water Studies Centre, School of Chemistry, Monash University, Australia, 3800

[3] CSIRO Oceans and Atmosphere, Hobart, Australia, 7000

*corresponding author, adam.kessler@monash.edu

Kessler, A. J., Roberts, K. L., Bissett, A. & Cook, P. L. M. (2018) Biogeochemical controls on the relative importance of denitrification and dissimilatory nitrate reduction to ammonium in estuaries. Global Biogeochem. Cycles 32, 1045–1057, doi:10.1029/2018GB005908

To view the published open abstract, go to http://dx.doi.org and enter the DOI.

Key Points:

- Dissolved iron and nitrate availability control the balance between denitrification and DNRA in estuaries
- Denitrification and DNRA rates in estuaries are of the same order of magnitude
- Most estuaries are slightly denitrification-dominant

Index terms
0469 Nitrogen cycling; 0442 Estuarine and nearshore processes; 0470 Nutrients and nutrient cycling;

Keywords

Denitrification; DNRA; Estuaries; Fe-DNRA

Abstract

The balance between estuarine denitrification and dissimilatory nitrate reduction to ammonium (DNRA) is critical for determining nitrogen loads received by oceans from inland waters. We aimed to determine the factors controlling the ratio between these processes and determining whether nitrogen was generally removed or recycled in estuaries. Rates of denitrification and DNRA with depth were measured in intact sediment cores in eleven estuaries along the coast of Victoria, Australia. The estuaries studied represent a range of biogeochemical conditions, land use and catchment size. At a pore-water profile scale, the ratio of denitrification to DNRA was well-predicted by a multiple regression model with nitrate concentration in the overlying water, dissolved pore water iron and ammonium as the predictor variables. Areal denitrification rates varied from 4 – 150 μmol m^{-2} h^{-1} and DNRA rates varied from 2 – 30 μmol m^{-2} h^{-1}, with the ratio of denitrification to DNRA spanning a range from denitrification-dominated (denitrification/DNRA = 8.4) to DNRA-dominated (denitrification/DNRA = 0.3). DNRA dominated at sites with high iron pools and high organic carbon to nitrate ratios. We conclude that low nitrate and high Fe^{2+} availability generally enhances DNRA and drives an estuary towards being N-recycling, rather than N-removing.

Introduction

Nitrogen is an important nutrient in natural waters controlling primary and secondary production and, as such, water body health and trophic status [*N Gruber and J N Galloway*, 2008]. Estuaries are important systems for the control of nitrogen cycling, as they receive the net nitrogen load from an entire catchment and connect it to the ocean [*D J Conley et al.*, 2009]. As nitrogen concentrations in global waters continue to rise as a result of human impact [*W Steffen et al.*, 2015], it is important to understand the factors that control the recycling or removal of nitrogen in all systems, and in particular in estuaries.

The major process by which nitrogen is removed from natural waters is denitrification – the stepwise reduction of nitrate or nitrite (NO_3^- or NO_2^-, together NO_x) to nitrogen gas (N_2) [*D E Canfield et al.*, 2005]. Conversely, dissimilatory nitrate reduction to ammonium (DNRA) reduces NO_x to ammonium (NH_4^+), which is usually retained in the system and remains bioavailable [*A E Giblin et al.*, 2013].

The major controls on the balance between denitrification and DNRA include availability of NO_x, temperature, organic carbon loading and availability of reductants. Under low or intermittent NO_x conditions, DNRA tends to outcompete denitrification, mostly due to the thermodynamic favourability of DNRA [*D Nizzoli et al.*, 2010]. Lower temperatures generally favour denitrification *in situ* [*R Gruca-Rokosz et al.*, 2009], and in laboratory experiments denitrifiers are found to have greater affinity for NO_x at temperatures below ~ 10 °C [*D King and D B Nedwell*, 1985; *B Ogilvie et al.*, 1997], although rates of both denitrification and DNRA increase with temperature [*A J Veraart et al.*, 2011]. The control by organic carbon loading and/or availability of reductants depends on the relative contribution to DNRA by heterotrophic and chemoautotrophic ammonifiers. Heterotrophic DNRA is favoured by high organic carbon loading, though reports of this process in estuaries are few,

and it is mostly observed in soils [*É Fazzolari et al.*, 1998; *S Yin et al.*, 2002]. Chemoautotrophic DNRA, conversely, depends on the availability of a reductant, usually assumed to be sulphide [*R Brunet and L Garcia-Gil*, 1996]. As such, the presence of sulphide can decrease the denitrification/DNRA through two means (1) by enhancing DNRA and (2) through sulphide inhibition of denitrification [*A J Burgin and S K Hamilton*, 2007].

Recently, a relationship between DNRA and dissolved iron (herein Fe^{2+}), whereby Fe^{2+}-enriched sediment decreased the ratio of denitrification to DNRA (denitrification/DNRA) from ~10 to ~2, was observed via slurry experiments in an estuarine environment [*E K Robertson et al.*, 2016]. The authors proposed a direct, energetically favourable, mechanism whereby Fe^{2+} is used as the reductant for DNRA [*E K Robertson et al.*, 2016]. Evidence for this metabolism had previously been observed in cultures of freshwater nitrate-reducing bacteria [*A J Coby et al.*, 2011; *K A Weber et al.*, 2006] and the above slurry experiments have since been performed with similar results in freshwater lakes [*E K Robertson and B Thamdrup*, 2017]. The broader relevance of this reaction in an estuarine context is, however, unknown.

With this in mind, we measured rates of denitrification and DNRA in eleven estuaries along the coast of Victoria, Australia using intact core incubations. In addition, putative denitrification and/or DNRA controlling variables were measured. We hypothesised that denitrification/DNRA would be controlled by nitrate concentration and dissolved iron (Fe^{2+}) such that lower nitrate and higher Fe^{2+} would favour DNRA and thus decrease denitrification/DNRA, leading to recycling of nitrogen within estuaries

Methods

Eleven estuaries were sampled along the coast of Victoria, Australia during July and August 2017 (Table 1, Fig 1). At each site, samples were collected from the main basin of the estuary, which we defined as the deepest, central muddy area of the estuary. Areas of the estuary with permeable sediment were avoided due to the complex transport regime in such sediments [*M Huettel et al.*, 1998] and the difficulty in recreating this reliably ex situ [*P L Cook et al.*, 2007]. As such, the sites provide an excellent range of environments for measuring the environmental influences on nitrogen cycling, but may not be accurately up-scalable to whole-estuary rates, however, this was not the aim of the study. The estuaries visited were chosen to span a range of geography, land use and catchments (Table 1).

Sample collection

At each sampling location, profiles of water column O_2, salinity and temperature were measured using a Hydrolab (DS5X) multiprobe sonde. Bottom water was collected by pump and filtered through a pre-combusted GFF filter for chlorophyll-*a* analysis. A total of 11 sediment cores were collected at each site in 6.6 cm ID polyethylene tubes and stoppered. Four of these were sieved through a 0.5 mm mesh and fauna was collected and counted. Fauna were preserved in ethanol and later identified to the family or genus level using local resources [*P L Beesley et al.*, 2000; *C Glasby and K Fauchald*, 2003; *S J Grove*, 2012; *A J Hirst*, 2004; *G Mapstone*, 1986; *G C Poore*, 1982]. The remaining seven cores were returned to the laboratory and transferred to a temperature controlled water bath and stirred with a magnetic stirrer suspended ~ 2 cm above the sediment surface.

Core incubations

Six sediment cores were left in the water bath overnight (~ 12-18 hours) before incubation to allow for re-equilibration, the seventh core was used to determine porosity as described below. Cores were left uncapped for every site except for MAL, which possessed near anoxic bottom-water. For every other site, O_2 remained steady at > 50% air saturation during this period and within 20-30% of in situ concentrations (see Table S1). The following day, $^{15}NO_3^-$ was added to the overlying water to a final concentration of 50 µM. Cores were topped up with ~ 20 ml of site water and capped with rubber stoppers ensuring no headspace inside the core, with the stirrer remaining in place. At each of 0, 1, 2, 3, 5 and 8 h after $^{15}NO_3^-$ addition, a single core was uncapped, and a sample for N_2 analysis was collected in a 12.5 mL glass vial (Labco Exetainer) and preserved with 0.25 mL of 50 % w/v $ZnCl_2$. A further 12 mL was filtered through a 0.22 µm syringe filter (Sartorius Minisart) into a polypropylene vial and frozen for later nutrient analysis.

The core was then extruded using a custom-built tool to push the bottom bung through the core liner, and sliced at depths of 0-0.5 cm, 0.5-1 cm, 1-2 cm, 2-3 cm, 3-5 cm and 5-10 cm below the sediment surface. These slices were then sampled to measure the fate of the $^{15}NO_3^-$ tracer and/or sediment geochemistry as described in Table 2.

For ^{15}N label samples, half of the slice was transferred to a pre-weighed beaker containing 2 % w/v $ZnCl_2$. The sample was gently stirred to homogenise, then quickly and carefully poured into a 12.5 ml exetainer and capped for ^{15}N-N_2 analysis. A further 6 mL of the sediment-$ZnCl_2$ slurry was subsequently frozen for the analysis of $^{15}NH_4^+$.

For sediment geochemistry samples, the remaining half slice was quickly transferred to a 50 mL centrifuge tube (Falcon) with a cap containing a butyl rubber septum. The tubes were immediately purged with Ar for > 2 minutes and then centrifuged at 4000 rpm for 10 minutes. The supernatant pore water was filtered through a 0.22 µm syringe filter and frozen for the analysis of NO_x and NH_4^+. A 0.5 mL subsample of this was then transferred to polypropylene vial already containing 0.5 mL of 0.01M Ferrozine for analysis of Fe^{2+} in the pore water. 0.5 g of the remaining sediment was

accurately weighed into a separate 50 mL centrifuge tube, to which 10 mL of Ar-purged ascorbate solution was added (2% ascorbic acid, 5% sodium citrate, 5% $NaHCO_3$ [*J E Kostka and G W Luther*, 1994; *T R Scicluna et al.*, 2015]). The tube was capped and purged with Ar for a further > 2 minutes, then shaken at 300 rpm for 24 h, then centrifuged at 4000 rpm for 10 minutes and sampled for Fe in the same manner as described for pore water. The iron in this pool is denoted Fe^{asc} is nominally referred to as the reactive, bioavailable iron [*J E Kostka and G W Luther*, 1994; *T R Scicluna et al.*, 2015]. The remaining sediment was frozen for later analysis of acid volatile sulphide and organic carbon.

Sample analysis

^{15}N-N_2 was analysed after introduction of a He headspace using a Sercon 20–22 continuous flow isotope ratio mass spectrometer (IRMS) coupled to a gas chromatograph (GC). $^{15}NH_4^+$ was extracted by 1:1 addition of 2 M KCl and shaken at 120 rpm for 1 hour, and was then transferred to a gas tight exetainer, purged with He to remove residual N_2 and the NH_4^+ converted to N_2 using 200 µL of alkaline hypobromite [*N Risgaard-Petersen et al.*, 1995] and analysed by GC-IRMS.

Nutrient samples were analysed for NO_x ($NO_x = NO_2^- + NO_3^-$), NH_4^+ and/or filterable reactive phosphorus (FRP) using standard colorimetric methods [*American Public Health Association*, 2005] on a Lachat Quickchem 8000 Flow Injection Analyser (FIA). All analyses were checked against a commercial SRM (ERA simple nutrients). Overlying water samples from the cores were analysed for NO_x, NH_4^+ and FRP. Pore water was analysed only for NH_4^+ and FRP due to limited sample volume.

Iron was analysed using the Ferrozine method [*E Viollier et al.*, 2000]. Samples were diluted until they fell within a 0 – 1 mg L^{-1} standard curve. As the majority of the pore water iron is assumed to be Fe(II), the sodium acetate and hydroxylamine hydrochlorite additions were made on all samples. Acid volatile suphide (AVS) was analysed using the rapid method described by *G Batley and S*

Simpson [2016]. Briefly, frozen sediment was thawed and homogenised in a glove box under an N2 atmosphere. Sediment (~ 0.1 g) was smeared using a PTFE-coated spatula onto a pre-weighed sheet of paraffin film then weighed and quickly transferred to a 50 mL centrifuge tube. 50 mL deoxygenated ultra-pure water and 5 mL Methylene Blue reagent [*S Fonselius et al.*, 2007] were added and the sample was inverted 5 times to mix. The sample was then removed from the glove box, centrifuged for 2 min at 2500 rpm and kept in the dark for 90 minutes before analysis by UV-visible spectrophotometry at 670 nm [*G Batley and S Simpson*, 2016; *S Fonselius et al.*, 2007]. Total Organic Carbon was determined by dry mass by weighing 30 mg of dried sediment into silver capsules. Inorganic carbon was removed by adding drops of 1 M HCl until no effervescence was observed. The dried samples were then analysed using an elemental analyser (Elementar Cube) and measured as % dry mass.

Porosity was measured by drying samples from the final sediment core collected at each site, except at LKN (assumed 0.84 per *T R Scicluna et al.* [2015]) and LW (assumed 0.75). All sediment concentrations were corrected for site porosity and are reported per litre of total sediment.

<u>Determination of denitrification and DNRA</u>

The rate of denitrification or DNRA at each depth in the measured profiles was determined by regressing the total excess ^{15}N as N_2 and NH_4^+ measured in each slice against time. No outliers were removed (see discussion). All sediment rates were corrected for site porosity and are reported per litre of total sediment.

For integrated (areal) rates, the excess $^{29}N_2$ and $^{30}N_2$ from both the denitrification and DNRA measurements were integrated through the core including the overlying water. These concentrations (in µmol m^{-2} were used to determine production rates of $^{29}N_2$ and $^{30}N_2$ and in turn the $^{14}N_2$ production rates (D_{14}) following standard isotope paring calculations [*L P Nielsen*, 1992]. For

DNRA calculations, the rate of $DNRA_{14}$ the reduction of $^{14}NO_x$ and $^{15}NO_x$ was assumed equal for both DNRA and denitrification [*N Risgaard-Petersen et al.*, 1995]. Rates are presented as µmol L^{-1} h^{-1} using total sediment volume. Note that this is equivalent to nmol mL^{-1} h^{-1} used in some literature.

Statistical approach

All data were fitted with linear regression models using the statistical package R (version 3.2.0) generally following the approach outlined for multiple regression by *M J Crawley* [2012]. Individual rates of D_{15} and $DNRA_{15}$ were first calculated by regressing the measured ^{15}N against time. A maximum-likelihood modelling approach was then used to determine the simplest adequate model (i.e., the best fit with the fewest predictor variables) for denitrification, DNRA, the ratio denitrification/DNRA and the per-site ratio denitrification/DNRA. Predictor variables used are shown in Table 3. Curvature was accounted for by log transformations of the response variables after checking for homogeneity and normality of variance graphically [*M J Crawley*, 2012]. The best model was identified using the Bayesian Information Criterion (BIC), which gives a conservative best model for a small dataset [*R E Kass and A E Raftery*, 1995]. It should be noted that this methodology predicts the most likely model to describe the (unknown) global dataset, and that this will almost certainly differ from the best predictive model (a model with a high R^2 good for interpolating). Akaike's Information Criterion corrected for small sample size (AICc) was also calculated, and this provided similar results. Where applicable, R^2 values are presented as R^2_{adj} – a parameter which penalises the addition of extra predictor variables (and thus minimises spurious models). Generally, the R^2_{adj} is much lower than the R^2 for a given regression, and while R^2 will always increase as extra predictor variables are added, R^2_{adj} only increases if the added term increases model predictive power above chance, and can be negative. As such, it serves as a similar metric as BIC and AICc.

Results

Water quality and physical parameters

Tables S1 and S2 show an overview of the water quality (WQ) parameters from the eleven estuaries. The sites visited varied in depth from 1.5 to 8 m, with bottom water salinity ranging from almost fresh (1.5) to saline (36.4). All sites were well aerated at the surface, but bottom water ranged from aerated (PAT) to almost anoxic (MAL), with a weak negative correlation between bottom water O_2 saturation and depth ($R^2 = 0.562$, $p < 0.01$). Bottom water temperature was generally similar between sites (8.3 – 13.9 °C), with a tendency to increase with water depth ($R^2 = 0.40$, $p < 0.05$). Chl-*a* concentrations ranged from below detection to 4.2 µg L^{-1} in the bottom water at TAM. Nutrient concentrations varied by approx. two orders of magnitude over the sites. At the more pristine sites TAM, WIN and MAL, $[NO_x]_{OW}$ and $[FRP]_{OW}$ were generally ≤ 1 µmol L^{-1}, while $[NH_4^+]_{OW}$ varied from 6.6 – 67 µmol L^{-1} at these sites. Elsewhere, $[NO_x]_{OW}$ varied from 3.4 to 49 µmol L^{-1}, with no clear relationship to $[NH_4^+]_{OW}$ or $[FRP]_{OW}$. This means that the 50 µmol L^{-1} additions of $^{15}NO_3^-$ used in this study represented enrichments of 2 × to 100 × *in situ* concentrations.

Sediment carbon was generally homogenous over the 10 cm at each site. PAT, LW and WER were the only two sites with [C] of < 2%, while WIN had > 8 % organic carbon (dry weight) at every depth analysed. AVS was not observed at any depth at AIR or PAT, or in the surface 2 cm at LW. All other sites had appreciable AVS in the surface 0.5 cm (10-50 mmol L^{-1}) increasing with depth to 50-200 mmol L^{-1}.

Faunal counts are available in the supplementary information (Table S3). In general, the fauna detected were dominated by polychaetes, in particular spionids and capitellids. HOP was the only site where no fauna were present in the four cores analysed. At AIR, YAR and MAL, < 20 individuals were counted (< ~ 1400 m^{-2}) and as a result bioirrigation is expected to be low at these sites. At all other sites 58-230 individuals (~ 4000 – 17000 m^{-2}) were counted.

238

239 Rates of denitrification and DNRA in individual slices

240 Figure 2 shows the profiles of denitrification rates measured in the eleven estuaries. In general, the
241 rate in the surface 0.5 cm was always ~ 1-3 μmol L^{-1} h. In most cases, denitrification was measurable
242 down to 2 cm below the SWI, and in many cases – in particular sites with high faunal abundance –
243 denitrification was seen as deep as the 5-10 cm layer. Measured DNRA rates (Figure 3) followed
244 similar trends, although the surface rate never exceeded 2 μmol L^{-1} h^{-1}. At AIR, MAL, PAT and WER,
245 the denitrification rate generally exceeded DNRA (Figure 4). At other sites the rates were either
246 similar, or slightly dominated by DNRA. In general, Figures 2-4 show both denitrification and DNRA
247 decrease with depth, and combining the data from each supports this with a broadly exponential
248 decay (see Figure S1 and later discussion).

249 Only those slices where the rate of D_{15} and/or $DNRA_{15}$ was larger than the error in the regression (i.e.
250 those rates which were statistically different from zero) were used in the regression analysis. Table 4
251 shows the best model found for D_{15}, $DNRA_{15}$ and the ratio $D_{15}/DNRA_{15}$.

252

253 Areal rates of denitrification and DNRA over sites

254 Figure 5 shows the areal rates of D_{14} calculated for each of the eleven estuaries. Figure 5c shows the
255 ratios $D_{14}/DNRA_{14}$ calculated for each site. Most sites are dominated by denitrification, except for
256 YAR and MAL, which slightly favour DNRA, and HOP, where DNRA exceeds denitrification by a factor
257 of 3. Figure 6 plots the rates in Figure 5 against a variety of sediment and water measurements.
258 Notably, D_{14} is positively correlated with AVS, and may also be correlated with Fe^{2+} and overlying NO_x
259 if WER is removed from the regression. $DNRA_{14}$ is also correlated with these parameters.

Discussion

Methodological considerations

In some systems, anaerobic ammonium oxidation (anammox) is thought to contribute a large proportion of NO_x removal [*M M Kuypers et al.*, 2003]. In this study we exclude any contribution from anammox as previous work at YAR [*K L Roberts et al.*, 2012] and LKN (Roberts unpubl.) have shown this pathway to account for < 1% of NO_x removal in Victorian estuaries. A study of 40 sites in 9 estuaries by *J C Nicholls and M Trimmer* [2009] showed that only 11 of these sites had annamox ratios *ra* > 9. Further, these 11 high-anammox sites had extremely high bottom water nitrate concentrations – on average 218 µM. If the sites in *J C Nicholls and M Trimmer* [2009] are limited to the 17 sites with bottom water nitrate less than 48 µM – the highest concentration in the present study – anammox was on average 2% of N_2 gas production, and therefore not likely significant. The ratio denitrification/DNRA could be interpreted as N removed/N recycled, and this does not significantly change the findings of this study. In this case, the following discussion could be interpreted as "predictors for N removal in estuaries", however as we expect anammox to be negligible, we refer to this as "denitrification" herein. We did not measure N_2O production during denitrification, as this typically accounts for < 1% of total denitrification even sites with high N_2O fluxes [*T Usui et al.*, 2001].

For the slice-specific rates D_{15} and $DNRA_{15}$, the rates presented are rates of $^{15}NO_x$ reduction and are therefore best interpreted as potential rates, rather than *in situ* relevant rates. We note that these could be converted to true rates (where $D_{14}^{slice} = D_{15}^{slice} \times [p_{29}^{slice}/(2\times p_{30}^{slice})]$), but this would be spurious use of the isotope pairing calculations, and in any case this would not affect the ratio, as $D_{14}^{slice}/DNRA_{14}^{slice} \equiv D_{15}/DNRA_{15}$. Note that once integrated through the core, the measurement is similar to homogenising an entire core and measuring the average production, which is the standard approach for isotope pairing [*L P Nielsen*, 1992]. Therefore, we convert only the integrated rates to true rates (D_{14} and $DNRA_{14}$), which are more representative of the ambient nitrate-reducing capacity.

285 Further, we note that between 20% and 48% of the recovered $^{15}N_2$ and 7% to 46% of the recovered
286 $^{15}NH_4^+$ was found in the overlying water, so these slice-specific ratios are, as such, only general
287 estimates. Addition of excess nitrate to sediment with high humic material can cause a cation
288 exchange effect where freshly formed $^{15}NH_4^+$ from DNRA is displaced by existing $^{14}NH_4^+$, causing a
289 nitrate induced ammonium flux [*W S Gardner et al.*, 2006]. As we consider both the pore water and
290 adsorbed NH_4^+ through our KCl extractions, this is not an issue for this study.

291 The method of measuring sedimentary denitrification in slices by placing the slice in $ZnCl_2$ and
292 quickly stirring and sealing is novel in this context. We acknowledge that we may be slightly
293 underestimating the denitrification rate due to loss of ^{15}N-N_2 during this process, but we believe this
294 to be minimal as the exposure time is very short (< 1 min). Previous work measuring denitrification
295 rates using diffusive equilibrium in thin gels (DET) showed that exposure of a 2.5 mm gel containing
296 4.4 µmol L^{-1} ^{15}N-N_2 for 1 min resulted in ~10% loss of gas, and that exposure for 20 minutes never
297 resulted in more than 25% loss [*A J Kessler et al.*, 2013]. Only two of the 330 slurries in the current
298 experiment had a concentration above 4.4 µmol L^{-1}, and exposure was < 1 min. Additionally, while
299 there was some exchange caused by stirring the sample, the sample depth was much greater than
300 2.5 mm (usually ~ 3 cm in the beaker), so the interface for N_2 loss was small. As such, we expect the
301 underestimation of ^{15}N-N_2 to be significantly less than 10%.

302 Rates of denitrification and DNRA are measured by individual regressions of excess ^{15}N
303 concentration against time. As the cores are unaltered environmental samples, natural
304 heterogeneity in sediment characteristics, nutrient distributions and especially faunal abundance
305 and bioirrigation result in large uncertainty around several of these regressions. Nonetheless, an
306 appreciable number of the denitrification (46/66) and DNRA (41/66) slices showed significant rates.
307 We refrained from the temptation to remove outlier points in these regressions (except for one core
308 from TAM, which was constantly enriched with $^{15}N_2/^{15}NH_4^+$ ~3 × higher than expected) as we believe
309 these outliers to represent true uncertainty due to between-core heterogeneity, and the “average”

rate of these samples. Whilst we had a good range of predictor variables available, we note a few measurements missing from this analysis. Pore water NO_x would have been an excellent measurement, however at the low concentrations and low sample volume possible, we were not able to measure this on our equipment. In any case, in previous experiments we have found NO_x to be below our detection limit even in zones of high denitrification and/or DNRA activity, as the transport rate is comparable to consumption rates and there is negligible accumulation. As both denitrification and DNRA are calculated by linear regression, the significant production rates reported are at steady state. Similarly, we were not able to measure pore water sulphide, but we treat AVS as a measure of highly reduced conditions. Finally, slice-by-slice fauna measurements, or tracer measurements in each core to determine depth-specific bioirrigation, may have helped us to explain some of the patterns observed e.g., in Figure 4, however this was not possible with the method used.

Slice-specific rates of D_{15} and $DNRA_{15}$

Each of D_{15} and $DNRA_{15}$ depend on depth (Table 4; see also Figure S1). There are several factors that may control this. Transport limitation and reaction near to the surface will obviously limit the rates at depth, as would be expected in situ, though as the majority of slices showed significant linear rates (Figures 2-4), these rates were steady-state (see previous paragraph). Additionally, carbon quality is likely diminished with depth, with more fresh, labile organic matter (LOM) near the surface and likely more refractory organic matter at depth [*E Kristensen*, 2000]. LOM will more easily serve as an electron donor for both denitrification and heterotrophic DNRA, and as it is consumed, increasingly refractory carbon is likely buried [*W S Gardner et al.*, 2017]. Unfortunately, we do not have either a direct measurement of carbon quality, or enough measurements of biological oxygen demand (BOD) as a proxy. However the profiles of organic carbon are very constant (Figure S2, Table S4), so it is probable that most LOM is quickly turned over in these systems, and that most carbon

335 remaining is relatively refractory. We also note that bioturbation, not quantified in this study, may
336 be responsible for the homogeneity in organic carbon. This is supported by MAL, the only site with
337 no fauna observed, having the least homogenous carbon profile (Figure S2).

338 In general, faunal abundance was not found to be a good predictor of denitrification or DNRA rates,
339 although the dependence on log(d_{sed}) is related to decreasing transport of NO_3^- to deeper sediment
340 layers, which in turn is related to bioirrigation rates. We did not attempt to quantify a potential
341 bioirrigation rate based on the size or behaviour of the observed faunal species, though we note that
342 our most abundant annelid families, spionidae [*C O Quintana et al.*, 2011; *J R Renz and S Forster*,
343 2013] and capitellidae [*L A Nickell et al.*, 2003; *R Przeslawski et al.*, 2009], are known irrigators and
344 many molluscs are known bioturbators [*E Kristensen et al.*, 2012]. A full analysis of the species
345 involved in bioirrigation and their relative effects on biogeochemical cycling is beyond the scope of
346 this study. While increased transport of nitrate to deeper slices will clearly enhance denitrificaiton
347 and/or DNRA, it is probable that this will also affect the sediment biogeochemistry and that this
348 effect is described by one of the other terms in the regression. Due to the limited sample volume
349 available, we do not have measurements of pore water NO_x concentrations, but the significant rates
350 of ^{15}N denitrification at various depths in the sediment (Figure 2) over an 8-hour period strongly
351 suggest that transport to deeper layers is achieved via bioirrigation. Indeed, the only site with no
352 measured fauna (Table S3) has the shallowest measured denitrification profile (Figure 2).

353 Denitrification's positive relationship with AVS was unexpected. Free sulphide is known to inhibit
354 denitrification [*A J Burgin and S K Hamilton*, 2007] and can enhance chemoautotrophic DNRA [*R*
355 *Brunet and L Garcia-Gil*, 1996]. While AVS is not a direct measure of this, it is likely that it represents
356 the majority of the sulphide pool in these sediments, however we note that either Fe^{2+} and/or Fe^{asc}
357 was observed at every depth and in every site, suggesting that the iron pool may have been large
358 enough to completely titrate the available sulphide. If this is the case, chemoautotrophic DNRA (with

359 HS^- as the electron donor) may be inhibited and denitrification may dominate in highly reduced
360 conditions.

361 The strong dependence of DNRA on organic carbon (Table 4) is likely due to a dependence on the
362 reduction of NO_3^- to NO_2^-, which is mediated by the same respiratory process as the first (identical)
363 step in denitrification [*D E Canfield et al.*, 2005]. Further, increased organic loading likely created
364 more reducing conditions and may result in more HS^- or Fe^{2+} for DNRA. This is further evidence that
365 the homogeneity of carbon profiles is more likely related to bioturbation than a lack of labile carbon
366 (see previous section and Figure S2). The absence of Fe^{2+} (or AVS) from the best model suggests that
367 either Fe^{2+}-driven DNRA is not the dominant DNRA pathway, or alternatively another step such as
368 NO_2^- production is limiting, and hence this model does not reflect the DNRA mechanism.

369 The finding that NO_x and Fe^{2+} form part of the best model for the ratio of $D_{15}/DNRA_{15}$ is strong
370 support for our hypothesis that this ratio would increase with increasing nitrate, and decrease with
371 increasing Fe^{2+}. From this alone, it is not possible to ascribe any contribution of each term to either
372 of denitrification or DNRA. The increase of the ratio of $D_{15}/DNRA_{15}$ with NO_x is consistent with
373 previous studies showing that when NO_x is plentiful, denitrification dominates, while DNRA is more
374 competitive when NO_x is limited [e.g. *K S Jørgensen*, 1989; *D Nizzoli et al.*, 2010; *B Ogilvie et al.*,
375 1997; *T O Strohm et al.*, 2007; *S Yoon et al.*, 2015]. Fe^{2+} may inhibit denitrification [*H K Carlson et al.*,
376 2012], accounting for the decrease in $D_{15}/DNRA_{15}$ with Fe^{2+}. Conversely, DNRA driven by Fe^{2+} has
377 recently been shown in the Yarra River estuary (YAR) [*K L Roberts et al.*, 2014; *E K Robertson et al.*,
378 2016] and similar biogeochemistry has been observed in freshwater environments [*E K Robertson*
379 *and B Thamdrup*, 2017]. This suggests that dissolved iron may more generally favour DNRA, even if
380 Fe^{2+}-DNRA is not the predominant DNRA pathway. In this experiment, unlike in the slurry
381 experiments performed by *E K Robertson and B Thamdrup* [2017] and *E K Robertson et al.* [2016],
382 the sediments are intact and not amended with additional dissolved iron. We believe the negative
383 influence of ammonium concentration on the ratio represents increased DNRA with higher

384 respiration rates (and thus higher ammonification), and therefore more reducing conditions. While
385 nitrification was not measured, these highly reduced environments would not be expected to exhibit
386 high rates.

387

388 Areal rates of D_{14} and $DNRA_{14}$ and wider applicability

389 Figure 5 shows the areally integrated rates of denitrification and DNRA. Denitrification and DNRA
390 were generally of the same order of magnitude, and $D_{14}/DNRA_{14}$ varied from 0.3 to 8.4, consistent
391 with other studies showing similar rates or slight DNRA-dominance in estuarine environments [*L F*
392 *Dong et al.*, 2011; *R J Dunn et al.*, 2013; *R J K Dunn et al.*, 2012]. In general, these ratios fall between
393 the high $D_{14}/DNRA_{14}$ (>> 10) observed in freshwater systems [*N Molnar et al.*, 2013; *D Nizzoli et al.*,
394 2010; *J T Scott et al.*, 2008] but lower than ratios of << 0.2 seen for highly contaminated marine
395 settings such as fish or shellfish farms [*P B Christensen et al.*, 2000; *D Nizzoli et al.*, 2006]. The three
396 sites that were DNRA-dominated (HOP, YAR and MAL) were the sites with lowest fauna counts
397 (Table S3), but there was no significant correlation between $DNRA_{14}$ and fauna ($p > 0.05$, not shown).
398 While a statistical approach as used for the slice-specific rates above, is not appropriate for such a
399 small dataset (11 points) with so many potential predictors, a series of plots can be used to help to
400 qualitatively explain the nitrogen-cycling behaviour over these estuaries.
401 Figure 6 shows that D_{14} is closely correlated with the integrated AVS concentration in the surface 2
402 cm of sediment. This is an unexpected response, but may be explained if all free sulphide is titrated
403 as AVS, as discussed above. WER is a clear outlier on these data – especially for D_{14}, though it is not
404 clear whether it should be excluded from these analyses. If removed, D_{14} showed a clear increase
405 with NO_x, which might be expected, but also an increase with Fe^{2+}, which was not expected,
406 especially given the negative relationship seen for $D_{15}/DNRA_{15}$ above. Further sampling of
407 denitrification-dominated sites similar to WER could expand this dataset enough to determine if
408 WER should be treated as an outlier, but we have no *a priori* reason to exclude it.

DNRA, similarly, was well-predicted by both AVS and NO_x. That both D_{14} and $DNRA_{14}$ increase with AVS supports our earlier discussion that AVS in this study generally represents reducing environments and not sulphide availability.

D Nizzoli et al. [2010] found that sediments with a high organic carbon to nitrate ratio exhibited higher DNRA rates. Figure 6 shows that while neither D_{14} nor $DNRA_{14}$ correlated strongly with this ratio, both processes only occurred at high rates when there was relatively low $C/[NO_x]_{OW}$. The ratio $D_{14}/DNRA_{14}$ shows no strong correlations, but notably this ratio is never high (> 1.5) when sediment Fe^{2+} is greater than 400 µmol m^{-2} or $C/[NO_x]_{OW}$ is greater than 3. While only circumstantial, this serves as some evidence that DNRA more broadly may be enhanced by high organic carbon to nitrate ratio as suggested by *D Nizzoli et al.* [2010] and high Fe^{2+} as suggested by *K L Roberts et al.* [2014].

This work suggests that lower nutrient loads and reducing conditions cause an estuary to tend towards N-recycling rather than N-removing conditions. This is an important finding for watershed management, as it suggests that high nutrient-load estuaries will likely improve their N-removal efficiency, somewhat buffering against eutrophication. This is consistent with the conceptual model recently proposed by *W S Gardner et al.* [2017], who demonstrated a cycle where algal biomass following a bloom provides increased labile organic matter, contributing to those more eutrophied sites becoming more efficient at N removal. Interestingly, where that study found that the increased organic matter (as LOM) increased denitrification, the present findings show a relationship between DNRA and organic matter, although the overall behaviour of more contaminated sites favouring denitrification is the same. Although measured over a small number of estuaries along a relatively short coastline (~ 500 km straight line East-West), integrated denitrification (4 – 150 µmol m^{-2} h^{-1}) and DNRA rates (2 – 30 µmol m^{-2} h^{-1}) spanned an order of magnitude, with $D_{14}/DNRA_{14}$ of 0.3 to 8.4. Over this large range of conditions, we were able to support our hypothesis of Fe^{2+} and NO_x as key controls of the relative importance of denitrification and DNRA at a pore water scale. Integrated

435 rates, conversely, were best described by overlying electron acceptor availability. Interestingly,
436 temperature was not significantly correlated with denitrification or DNRA, although we note that our
437 site temperatures varied only by a few degrees, and were in the range reported as favourable to
438 DNRA [*B Ogilvie et al.*, 1997]. As such, we believe that the findings of this work are generally
439 applicable to a variety of estuaries, and that this work will be useful for monitoring and management
440 of nitrogen processing in estuaries globally. It is interesting that the parameter $[NO_x]_{OW}$ does not
441 include the 50 µmol L^{-1} $^{15}NO_3^-$ added to each core. This suggests that, at least on the timescale of ≤ 8
442 hours, initially nitrate-deplete systems will continue to act as such, even after a significant
443 concentration of nitrate is present. The time scale for such a system switching from net recycling
444 (DNRA-dominated) to net removing (denitrification-dominated) would make an interesting
445 continuation of this work.
446
447

Acknowledgements

We thank D Brehm, S Koh, W Wong and V Eate for assistance in the field and laboratory. This project was supported by Australian Research Council Discovery Program Grant DP150101281. All data are included as supplementary information to this article. We thank W Gardner and one anonymous reviewer for helpful comments which have improved this manuscript.

References

American Public Health Association (2005), *Standard methods for the examination of water and wastewater*.

Batley, G., and S. Simpson (2016), *Sediment quality assessment: a practical guide*, CSIRO PUBLISHING.

Beesley, P. L., G. J. Ross, and C. J. Glasby (2000), *Polychaetes & allies: the southern synthesis*, CSIRO publishing.

Brunet, R., and L. Garcia-Gil (1996), Sulfide-induced dissimilatory nitrate reduction to ammonia in anaerobic freshwater sediments, *FEMS Microbiology Ecology*, *21*(2), 131-138.

Burgin, A. J., and S. K. Hamilton (2007), Have we overemphasized the role of denitrification in aquatic ecosystems? A review of nitrate removal pathways, *Frontiers in Ecology and the Environment*, *5*(2), 89-96.

Canfield, D. E., E. Kristensen, and B. Thamdrup (2005), *Aquatic geomicrobiology*, Gulf Professional Publishing.

Carlson, H. K., I. C. Clark, R. A. Melnyk, and J. D. Coates (2012), Toward a mechanistic understanding of anaerobic nitrate-dependent iron oxidation: balancing electron uptake and detoxification, *Frontiers in microbiology*, *3*.

Christensen, P. B., S. Rysgaard, N. P. Sloth, T. Dalsgaard, and S. Schwærter (2000), Sediment mineralization, nutrient fluxes, denitrification and dissimilatory nitrate reduction to ammonium in an estuarine fjord with sea cage trout farms, *Aquatic microbial ecology*, *21*(1), 73-84.

Coby, A. J., F. Picardal, E. Shelobolina, H. Xu, and E. E. Roden (2011), Repeated anaerobic microbial redox cycling of iron, *Applied and environmental microbiology*, *77*(17), 6036-6042.

Conley, D. J., H. W. Paerl, R. W. Howarth, D. F. Boesch, S. P. Seitzinger, K. E. Havens, C. Lancelot, and G. E. Likens (2009), Controlling eutrophication: nitrogen and phosphorus, *Science*, *323*(5917), 1014-1015.

Cook, P. L., F. Wenzhöfer, R. N. Glud, F. Janssen, and M. Huettel (2007), Benthic solute exchange and carbon mineralization in two shallow subtidal sandy sediments: Effect of advective pore‐water exchange, *Limnology and Oceanography*, *52*(5), 1943-1963.

Crawley, M. J. (2012), *The R book*, John Wiley & Sons.

Dong, L. F., M. N. Sobey, C. J. Smith, I. Rusmana, W. Phillips, A. Stott, A. M. Osborn, and D. B. Nedwell (2011), Dissimilatory reduction of nitrate to ammonium, not denitrification or anammox, dominates benthic nitrate reduction in tropical estuaries, *Limnology and Oceanography*, *56*(1), 279-291.

Dunn, R. J., D. Robertson, P. R. Teasdale, N. J. Waltham, and D. T. Welsh (2013), Benthic metabolism and nitrogen dynamics in an urbanised tidal creek: Domination of DNRA over denitrification as a nitrate reduction pathway, *Estuarine, Coastal and Shelf Science*, *131*, 271-281.

Dunn, R. J. K., D. T. Welsh, M. A. Jordan, N. J. Waltham, C. J. Lemckert, and P. R. Teasdale (2012), Benthic metabolism and nitrogen dynamics in a sub-tropical coastal lagoon: Microphytobenthos stimulate nitrification and nitrate reduction through photosynthetic oxygen evolution, *Estuarine, Coastal and Shelf Science*, *113*, 272-282.

Fazzolari, É., B. Nicolardot, and J. C. Germon (1998), Simultaneous effects of increasing levels of glucose and oxygen partial pressures on denitrification and dissimilatory nitrate reduction to ammonium in repacked soil cores, *European Journal of Soil Biology*, *34*(1), 47-52.

Fonselius, S., D. Dyrssen, and B. Yhlen (2007), Determination of hydrogen sulphide, *Methods of Seawater Analysis, Third Edition*, 91-100.

Gardner, W. S., M. J. McCarthy, S. An, D. Sobolev, K. S. Sell, and D. Brock (2006), Nitrogen fixation and dissimilatory nitrate reduction to ammonium (DNRA) support nitrogen dynamics in Texas estuaries, *Limnology and Oceanography*, *51*(1part2), 558-568.

Gardner, W. S., S. E. Newell, M. J. McCarthy, D. K. Hoffman, K. Lu, P. J. Lavrentyev, F. L. Hellweger, S. W. Wilhelm, Z. Liu, and D. A. Bruesewitz (2017), Community biological ammonium demand: a conceptual model for cyanobacteria blooms in eutrophic lakes, *Environmental science & technology*, *51*(14), 7785-7793.

Giblin, A. E., C. R. Tobias, B. Song, N. Weston, G. T. Banta, and V. H. RIVERA-MONROY (2013), The importance of dissimilatory nitrate reduction to ammonium (DNRA) in the nitrogen cycle of coastal ecosystems, *Oceanography*, *26*(3), 124-131.

Glasby, C., and K. Fauchald (2003), POLiKEY Version 2, *Australian Biological Resources Study, Canberra*.

Grove, S. J. (2012), *Guide to the Seashells and Other Marine Molluscs of Tasmania*.

Gruber, N., and J. N. Galloway (2008), An Earth-system perspective of the global nitrogen cycle, *Nature*, *451*(7176), 293.

Gruca-Rokosz, R., J. A. Tomaszek, and P. Koszelnik (2009), Competitiveness of dissimilatory nitrate reduction processes in bottom sediment of Rzeszów reservoir, *Environ Protect Eng*, *35*, 5-13.

Hirst, A. J. (2004), Broad-scale environmental gradients among estuarine benthic macrofaunal assemblages of south-eastern Australia: implications for monitoring estuaries, *Marine and Freshwater Research*, *55*(1), 79-92.

Huettel, M., W. Ziebis, S. Forster, and G. Luther (1998), Advective transport affecting metal and nutrient distributions and interfacial fluxes in permeable sediments, *Geochimica et Cosmochimica Acta*, *62*(4), 613-631.

Jørgensen, K. S. (1989), Annual pattern of denitrification and nitrate ammonification in estuarine sediment, *Applied and Environmental Microbiology*, *55*(7), 1841-1847.

Kass, R. E., and A. E. Raftery (1995), Bayes factors, *Journal of the american statistical association*, *90*(430), 773-795.

Kessler, A. J., R. N. Glud, M. B. Cardenas, and P. L. M. Cook (2013), Transport zonation limits coupled nitrification-denitrification in permeable sediments, *Environmental Science & Technology*, *47*(23), 13404-13411.

King, D., and D. B. Nedwell (1985), The influence of nitrate concentration upon the end-products of nitrate dissimilation by bacteria in anaerobic salt marsh sediment, *FEMS Microbiology Ecology*, *1*(1), 23-28.

Kostka, J. E., and G. W. Luther (1994), Partitioning and speciation of solid phase iron in saltmarsh sediments, *Geochimica et Cosmochimica Acta*, *58*(7), 1701-1710.

Kristensen, E. (2000), Organic matter diagenesis at the oxic/anoxic interface in coastal marine sediments, with emphasis on the role of burrowing animals, in *Life at interfaces and under extreme conditions*, edited, pp. 1-24, Springer.

Kristensen, E., G. Penha-Lopes, M. Delefosse, T. Valdemarsen, C. O. Quintana, and G. T. Banta (2012), What is bioturbation? The need for a precise definition for fauna in aquatic sciences, *Marine Ecology Progress Series*, *446*, 285-302.

Kuypers, M. M., A. O. Sliekers, G. Lavik, and M. Schmid (2003), Anaerobic ammonium oxidation by anammox bacteria in the Black Sea, *Nature*, *422*(6932), 608.

Mapstone, G. (1986), *A Key to the Common Intertidal Organisms of Wilsons Promotory, Victoria, Australia*, La Trobe University.

Molnar, N., D. T. Welsh, C. Marchand, J. Deborde, and T. Meziane (2013), Impacts of shrimp farm effluent on water quality, benthic metabolism and N-dynamics in a mangrove forest (New Caledonia), *Estuarine, Coastal and Shelf Science*, *117*, 12-21.

Nicholls, J. C., and M. Trimmer (2009), Widespread occurrence of the anammox reaction in estuarine sediments, *Aquatic microbial ecology*, *55*(2), 105-113.

Nickell, L. A., K. D. Black, D. J. Hughes, J. Overnell, T. Brand, T. D. Nickell, E. Breuer, and S. M. Harvey (2003), Bioturbation, sediment fluxes and benthic community structure around a salmon cage farm in Loch Creran, Scotland, *Journal of Experimental Marine Biology and Ecology*, *285*, 221-233.

Nielsen, L. P. (1992), Denitrification in sediment determined from nitrogen isotope pairing, *FEMS Microbiology Letters*, *86*(4), 357-362.

Nizzoli, D., D. T. Welsh, E. A. Fano, and P. Viaroli (2006), Impact of clam and mussel farming on benthic metabolism and nitrogen cycling, with emphasis on nitrate reduction pathways, *Marine Ecology Progress Series*, *315*, 151-165.

Nizzoli, D., E. Carraro, V. Nigro, and P. Viaroli (2010), Effect of organic enrichment and thermal regime on denitrification and dissimilatory nitrate reduction to ammonium (DNRA) in hypolimnetic sediments of two lowland lakes, *Water Research*, *44*(9), 2715-2724.
Ogilvie, B., M. Rutter, and D. Nedwell (1997), Selection by temperature of nitrate‐reducing bacteria from estuarine sediments: species composition and competition for nitrate, *FEMS Microbiology Ecology*, *23*(1), 11-22.
Poore, G. C. (1982), Benthic communities of the Gippsland Lakes, Victoria, *Marine and Freshwater Research*, *33*(5), 901-915.
Przeslawski, R., Q. Zhu, and R. Aller (2009), Effects of abiotic stressors on infaunal burrowing and associated sediment characteristics, *Marine Ecology Progress Series*, *392*, 33-42.
Quintana, C. O., T. Hansen, M. Delefosse, G. Banta, and E. Kristensen (2011), Burrow ventilation and associated porewater irrigation by the polychaete Marenzelleria viridis, *Journal of Experimental Marine Biology and Ecology*, *397*(2), 179-187.
Renz, J. R., and S. Forster (2013), Are similar worms different? A comparative tracer study on bioturbation in the three sibling species Marenzelleria arctia, M. viridis, and M. neglecta from the Baltic Sea, *Limnology and Oceanography*, *58*(6), 2046-2058.
Risgaard-Petersen, N., N. P. Revsbech, and S. Rysgaard (1995), Combined microdiffusion-hypobromite oxidation method for determining nitrogen-15 isotope in ammonium, *Soil Science Society of America Journal*, *59*(4), 1077-1080.
Roberts, K. L., A. J. Kessler, M. R. Grace, and P. L. M. Cook (2014), Increased rates of dissimilatory nitrate reduction to ammonium (DNRA) under oxic conditions in a periodically hypoxic estuary, *Geochimica et Cosmochimica Acta*, *133*, 313-324.
Roberts, K. L., V. M. Eate, B. D. Eyre, D. P. Holland, and P. L. Cook (2012), Hypoxic events stimulate nitrogen recycling in a shallow salt‐wedge estuary: The Yarra River estuary, Australia, *Limnology and Oceanography*, *57*(5), 1427-1442.
Robertson, E. K., and B. Thamdrup (2017), The fate of nitrogen is linked to iron(II) availability in a freshwater lake sediment, *Geochimica et Cosmochimica Acta*, *205*(Supplement C), 84-99.
Robertson, E. K., K. L. Roberts, L. D. Burdorf, P. Cook, and B. Thamdrup (2016), Dissimilatory nitrate reduction to ammonium coupled to Fe (II) oxidation in sediments of a periodically hypoxic estuary, *Limnology and Oceanography*, *61*(1), 365-381.
Scicluna, T. R., R. J. Woodland, Y. Zhu, M. R. Grace, and P. L. Cook (2015), Deep dynamic pools of phosphorus in the sediment of a temperate lagoon with recurring blooms of diazotrophic cyanobacteria, *Limnology and Oceanography*, *60*(6), 2185-2196.
Scott, J. T., M. J. McCarthy, W. S. Gardner, and R. D. Doyle (2008), Denitrification, dissimilatory nitrate reduction to ammonium, and nitrogen fixation along a nitrate concentration gradient in a created freshwater wetland, *Biogeochemistry*, *87*(1), 99-111.
Steffen, W., K. Richardson, J. Rockström, S. E. Cornell, I. Fetzer, E. M. Bennett, R. Biggs, S. R. Carpenter, W. de Vries, and C. A. de Wit (2015), Planetary boundaries: Guiding human development on a changing planet, *Science*, *347*(6223), 1259855.
Strohm, T. O., B. Griffin, W. G. Zumft, and B. Schink (2007), Growth yields in bacterial denitrification and nitrate ammonification, *Applied and environmental microbiology*, *73*(5), 1420-1424.
Usui, T., I. Koike, and N. Ogura (2001), N2O production, nitrification and denitrification in an estuarine sediment, *Estuarine, Coastal and Shelf Science*, *52*(6), 769-781.
Veraart, A. J., J. J. M. de Klein, and M. Scheffer (2011), Warming Can Boost Denitrification Disproportionately Due to Altered Oxygen Dynamics, *PLOS ONE*, *6*(3), e18508.
Viollier, E., P. Inglett, K. Hunter, A. Roychoudhury, and P. Van Cappellen (2000), The ferrozine method revisited: Fe (II)/Fe (III) determination in natural waters, *Applied geochemistry*, *15*(6), 785-790.
Weber, K. A., M. M. Urrutia, P. F. Churchill, R. K. Kukkadapu, and E. E. Roden (2006), Anaerobic redox cycling of iron by freshwater sediment microorganisms, *Environmental Microbiology*, *8*(1), 100-113.

605 Yin, S., D. Chen, L. Chen, and R. Edis (2002), Dissimilatory nitrate reduction to ammonium and
606 responsible microorganisms in two Chinese and Australian paddy soils, *Soil Biology and*
607 *Biochemistry*, *34*(8), 1131-1137.
608 Yoon, S., C. Cruz-García, R. Sanford, K. M. Ritalahti, and F. E. Löffler (2015), Denitrification versus
609 respiratory ammonification: environmental controls of two competing dissimilatory
610 NO(3)(−)/NO(2)(−) reduction pathways in Shewanella loihica strain PV-4, *The ISME Journal*, *9*(5),
611 1093-1104.

612

613

Tables

Table 1: Estuaries used in this study. Shown for each are an abbreviated label used throughout the text, coordinates of the sampling point recorded using on-board GPS, a general description of the catchment based on predominant land use, percentage of catchment area fertilized (Fert%), population per km^2 of catchment area (Pop), and a Map ID to reference Fig 1.

Site name	Label	Coordinates	Description	Fert%	Pop	Map ID
Hopkins River	HOP	-38.401966, 142.542951	Agricultural	88.7	5.5	1
Curdies River	CUR	-38.576394, 142.872120	Agricultural	86.6	5.5	2
Aire River	AIR	-38.795289, 143.477458	Rural	14	1	3
Werribee River	WER	-37.947977, 144.664402	Urban	56.4	58.3	4
Yarra River	YAR	-37.834230, 145.025396	Urban	43.6	347	5
Patterson River	PAT	-38.066820, 145.137649	Urban	57.1	1003	6
Lake Wellington	LW	-38.096833, 147.314111	Rural	33	11.6	7
Lake King	LKN	-37.875333, 147.773694	Rural	14.7	2.5	8
Tamboon Inlet	TAM	-37.737517, 149.139686	Pristine	1.9	0.4	9
Wingan inlet	WIN	-37.718861, 149.498833	Pristine	0.5	0.09	10
Mallacoota Inlet	MAL	-37.482833, 149.692422	Pristine	2.9	0.3	11

Table 2: Core sampling procedure employed at each site.

Core	Time (h)	Pore water samples collected	Solid samples collected
1	0	Fe^{2+}, NH_4^+, FRP	Fe^{asc}, C, AVS
2	1	$^{15}N\text{-}N_2$, $^{15}NH_4^+$	
3	2	$^{15}N\text{-}N_2$, $^{15}NH_4^+$	
4	3	$^{15}N\text{-}N_2$, $^{15}NH_4^+$	
5	5	Fe^{2+}, NH_4^+, FRP $^{15}N\text{-}N_2$, $^{15}NH_4^+$	Fe^{asc}, C, AVS
6	8	Fe^{2+}, NH_4^+, FRP $^{15}N\text{-}N_2$, $^{15}NH_4^+$	Fe^{asc}, C, AVS

Table 3: Variables used in multiple regressions for slice-specific nitrogen processing rates. Also noted is whether the data are measured per site (n = 11) or per slice (n = 66). All concentrations are expressed as per total sediment volume.

Variable	**Description**	**Unit**	**Property**
$\ln(d_{sed})$	Depth in sediment (natural log)	cm	SLICE
T_{OW}	Bottom water temperature	°C	SITE
fert	Percentage of catchment area fertilized	%	SITE
$[Fe^{2+}]$	Sediment dissolved Fe concentration	µmol L^{-1}	SLICE
$[Fe^{asc}]$	Sediment ascorbate-extractible Fe concentration	µmol L^{-1}	SLICE
[AVS]	Acid volatile sulphide	µmol L^{-1}	SLICE
[C]	Organic carbon	mol L^{-1}	SLICE
$[NH_4^+]$	Sediment ammonium concentration	µmol L^{-1}	SLICE
F	Total fauna count	m^{-2}	SITE
$[NO_x]_{OW}$	Bottom water NO_x concentration	µmol L^{-1}	SITE
$[NH_4^+]_{OW}$	Bottom water ammonium concentration	µmol L^{-1}	SITE
DO_{OW}	Bottom water oxygen concentration	mg L^{-1}	SITE
$[chl\text{-}a]_{OW}$	Bottom water chlorophyll-*a* concentration	µg L^{-1}	SITE

Table 4: Best models for potential rates D_{15}, $DNRA_{15}$ and $D_{15}/DNRA_{15}$ in individual slices (n = 46, 41, 35) based on BIC.

					BIC	**AICc**	**p**	**R^2_{adj}**	**R^2**
$\ln(D_{15})$ =	–1.55	– 1.24 $\ln(d_{sed})$	+ 9.99 × 10^{-6} [AVS]		124	118	<< 0.001	0.746	0.757
$\ln(DNRA_{15})$ =	–2.60	– 0.931 $\ln(d_{sed})$	+ 41.8 [C]		110	105	<< 0.001	0.641	0.659
$\ln(D_{15}/DNRA_{15})$ =	0.188	– 0.000958 $[NH_4^+]$	+ 0.0444 $[NO_x]_{OW}$	– 0.00420 $[Fe^{2+}]$	84.7	79.0	<< 0.001	0.461	0.508

Figure Captions

Figure 1: Location of the 11 estuaries visited in this study

Fig 2: D_{15} rates (µmol L^{-1} h^{-1}) measured as $^{15}N_2$ accumulation as profiles from six slices (0-0.5 cm, 0.5-1cm, 1-2 cm, 2-3 cm, 3-5 cm, 5-10 cm) at each of the 11 estuaries studied. Error bars are ± 1 s.e. Grey points denote slices where the standard error of the regression is larger than the rate; these points are excluded from later statistical analysis.

Fig 3: $DNRA_{15}$ rates (µmol L^{-1} h^{-1}) measured as $^{15}NH_4^+$ accumulation as profiles from six slices (0-0.5 cm, 0.5-1cm, 1-2 cm, 2-3 cm, 3-5 cm, 5-10 cm) at each of the 11 estuaries studied. Error bars are ± 1 s.e. Grey points denote slices where the standard error of the regression is larger than the rate; these points are excluded from later statistical analysis.

Fig 4: the ratio $D_{15}/DNRA_{15}$ as profiles from six slices (0-0.5 cm, 0.5-1cm, 1-2 cm, 2-3 cm, 3-5 cm, 5-10 cm) at each of the 11 estuaries studied. Black points denote slices where both D_{15} and $DNRA_{15}$ are significant. White points show non-significant ratios where those ratios fall on the scale of 0 – 10, but these points are not considered in any further analysis. Some non-significant values (e.g. where non-significant $DNRA_{15}$ is very small) are outside of this range, and are not plotted. Vertical line shows $D_{15}/DNRA_{15} = 1$.

Fig 5: Areal rates of (a) D_{14} and (b) $DNRA_{14}$ at each estuary, and (c) the ratio $D_{14}/DNRA_{14}$. Horizontal line shows a ratio of 1.

Fig 6: Areal (integrated) rates of (a) D_{14} and (b) $DNRA_{14}$ at each estuary plotted against Fe^{2+} (µmol m^{-2}), AVS (mmol m^{-2}), overlying NOx concentration (µmol L^{-1}), mean organic carbon (% dry weight) and the ratio of organic carbon to overlying NOx (% d.w. / µmol L^{-1}). Fe^{2+} and AVS are integrated over the surface 2 cm at each site. Organic carbon is averaged over the surface 2 cm. In each plot, WER is highlighted in grey. The p value for an ANOVA of the regression of each plot is shown when significant ($p < 0.05$). Values in brackets denote that the regression is only significant when WER is excluded. Horizontal lines in the bottom panel shows a ratio of 1.

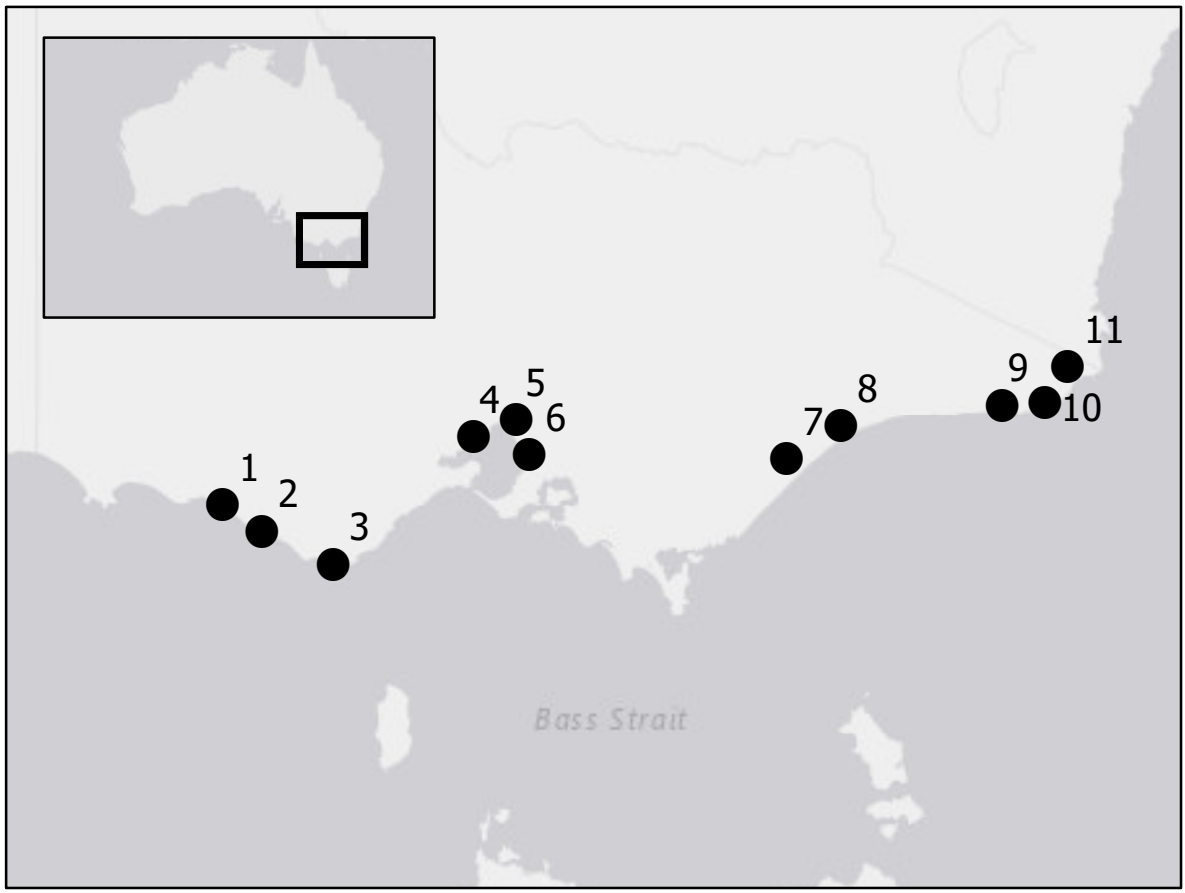
1
2
3
4
5
6
7
8
9
10
11
Bass Strait

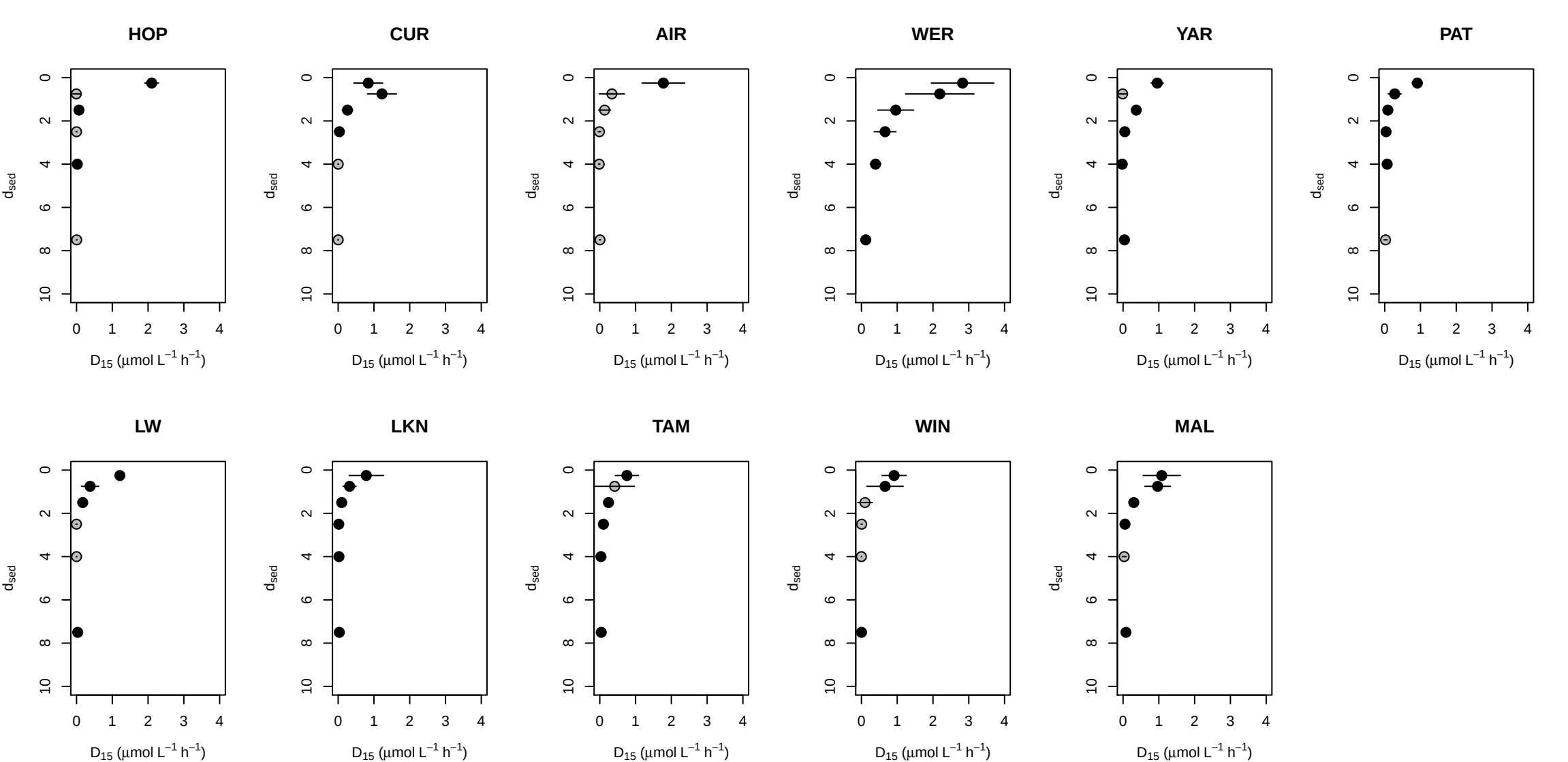
HOP
CUR
AIR
WER
YAR
PAT
LW
LKN
TAM
WIN
MAL
d_{sed}
D_{15} (µmol L^{-1} h^{-1})
0
1
2
3
4
0
2
4
6
8
10

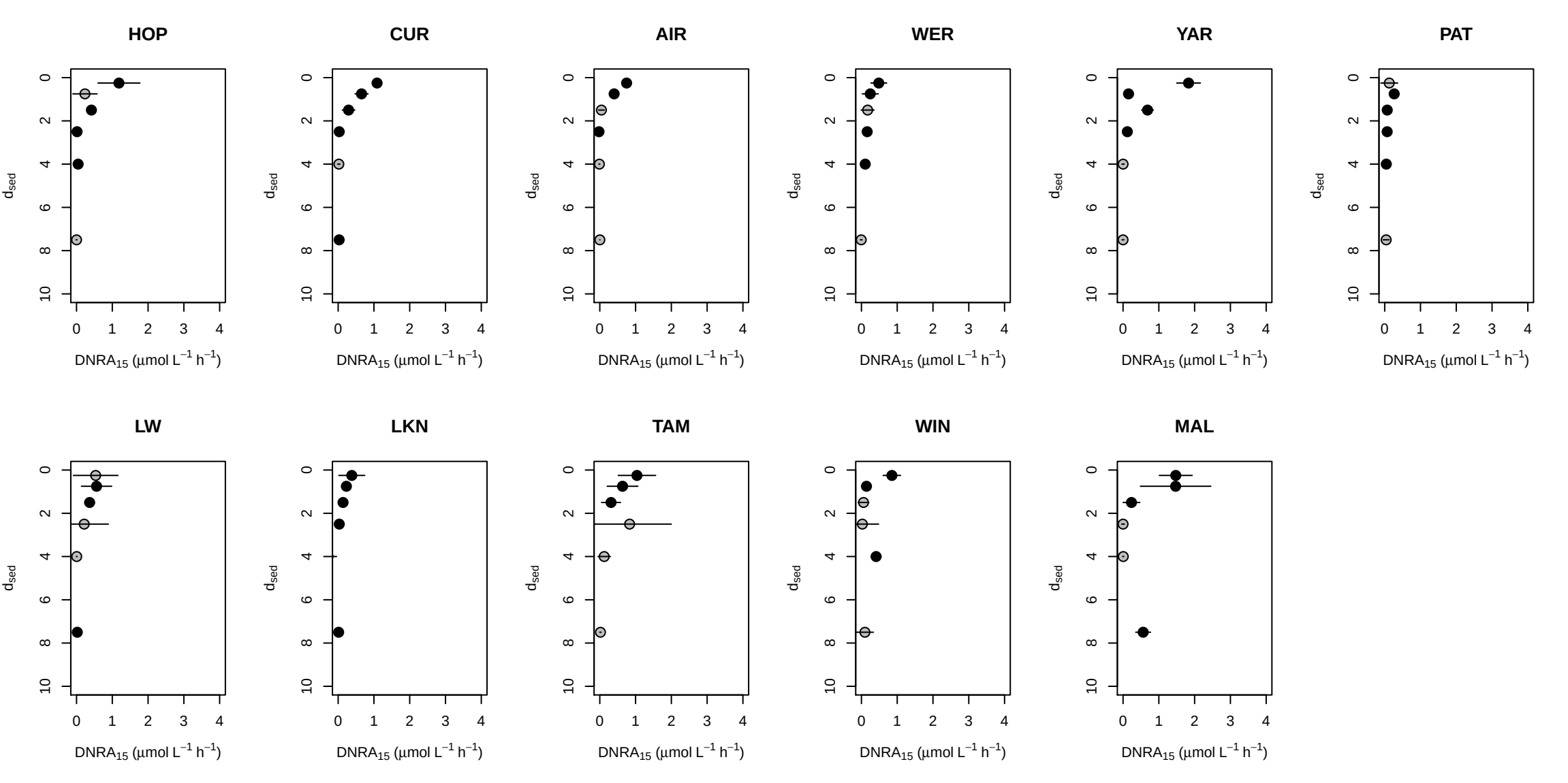
HOP
CUR
AIR
WER
YAR
PAT
LW
LKN
TAM
WIN
MAL
d_{sed}
0
2
4
6
8
10
0
1
2
3
4
$DNRA_{15}$ (µmol L^{-1} h^{-1})

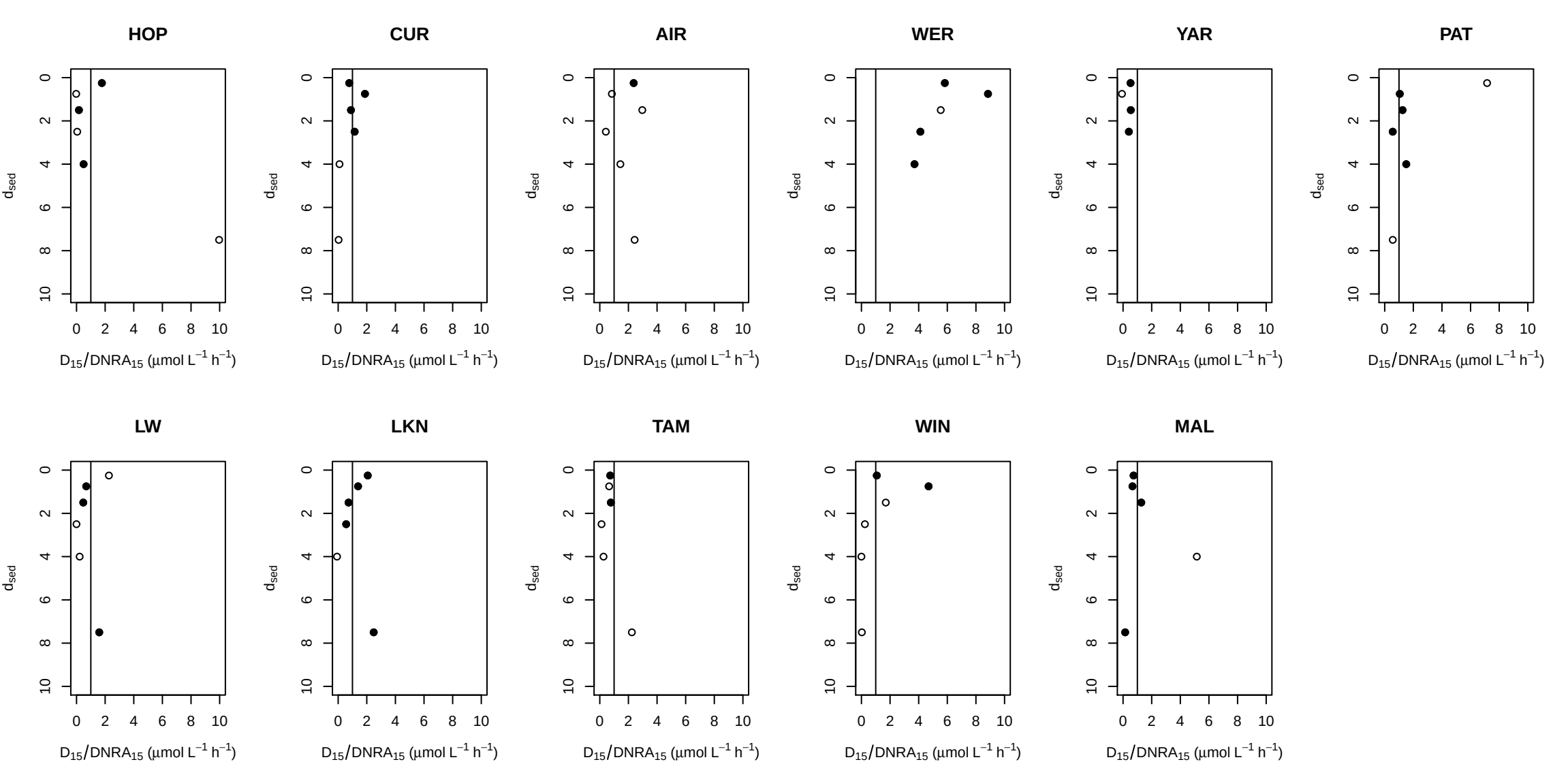
HOP
CUR
AIR
WER
YAR
PAT
LW
LKN
TAM
WIN
MAL
d_{sed}
$D_{15}/DNRA_{15}$ (µmol L^{-1} h^{-1})
0
2
4
6
8
10

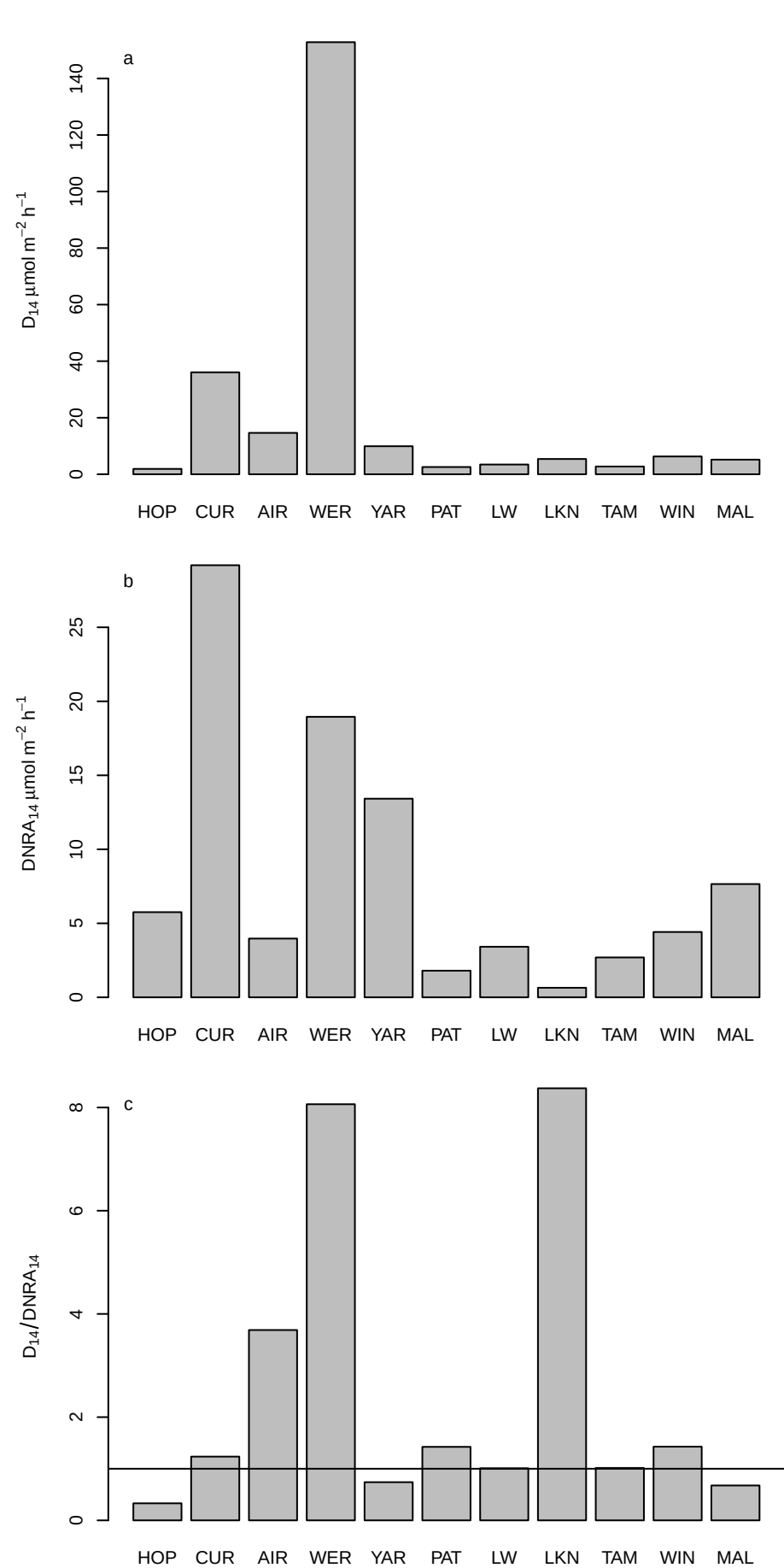
a
D_{14} µmol m^{-2} h^{-1}
0
20
40
60
80
100
120
140
HOP
CUR
AIR
WER
YAR
PAT
LW
LKN
TAM
WIN
MAL
b
$DNRA_{14}$ µmol m^{-2} h^{-1}
0
5
10
15
20
25
HOP
CUR
AIR
WER
YAR
PAT
LW
LKN
TAM
WIN
MAL
c
$D_{14}/DNRA_{14}$
0
2
4
6
8
HOP
CUR
AIR
WER
YAR
PAT
LW
LKN
TAM
WIN
MAL

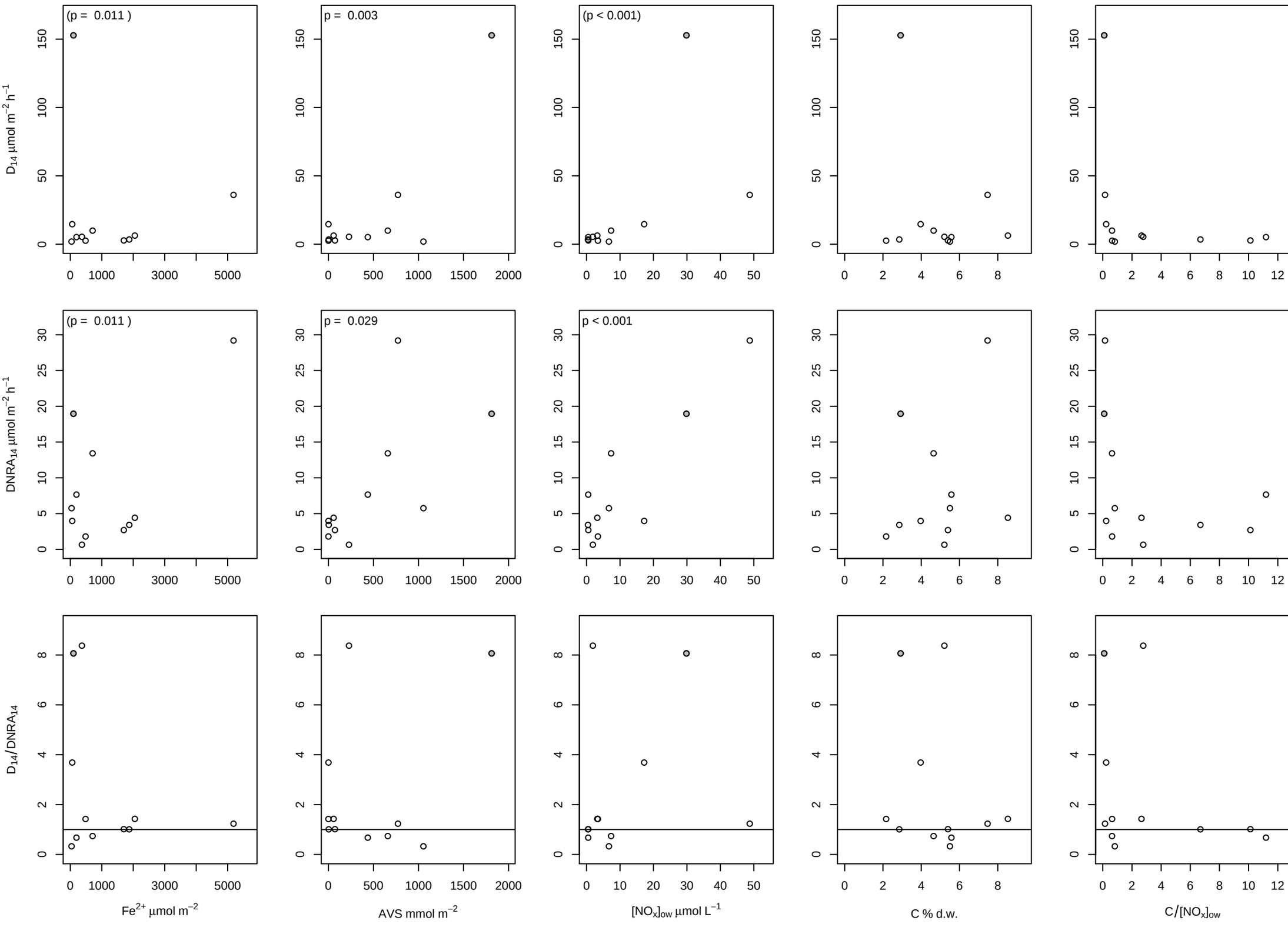
(p = 0.011)
p = 0.003
(p < 0.001)
(p = 0.011)
p = 0.029
p < 0.001
D14 µmol m−2 h−1
DNRA14 µmol m−2 h−1
D14/DNRA14
Fe2+ µmol m−2
AVS mmol m−2
[NOx]ow µmol L−1
C % d.w.
C/[NOx]ow

Supplementary information

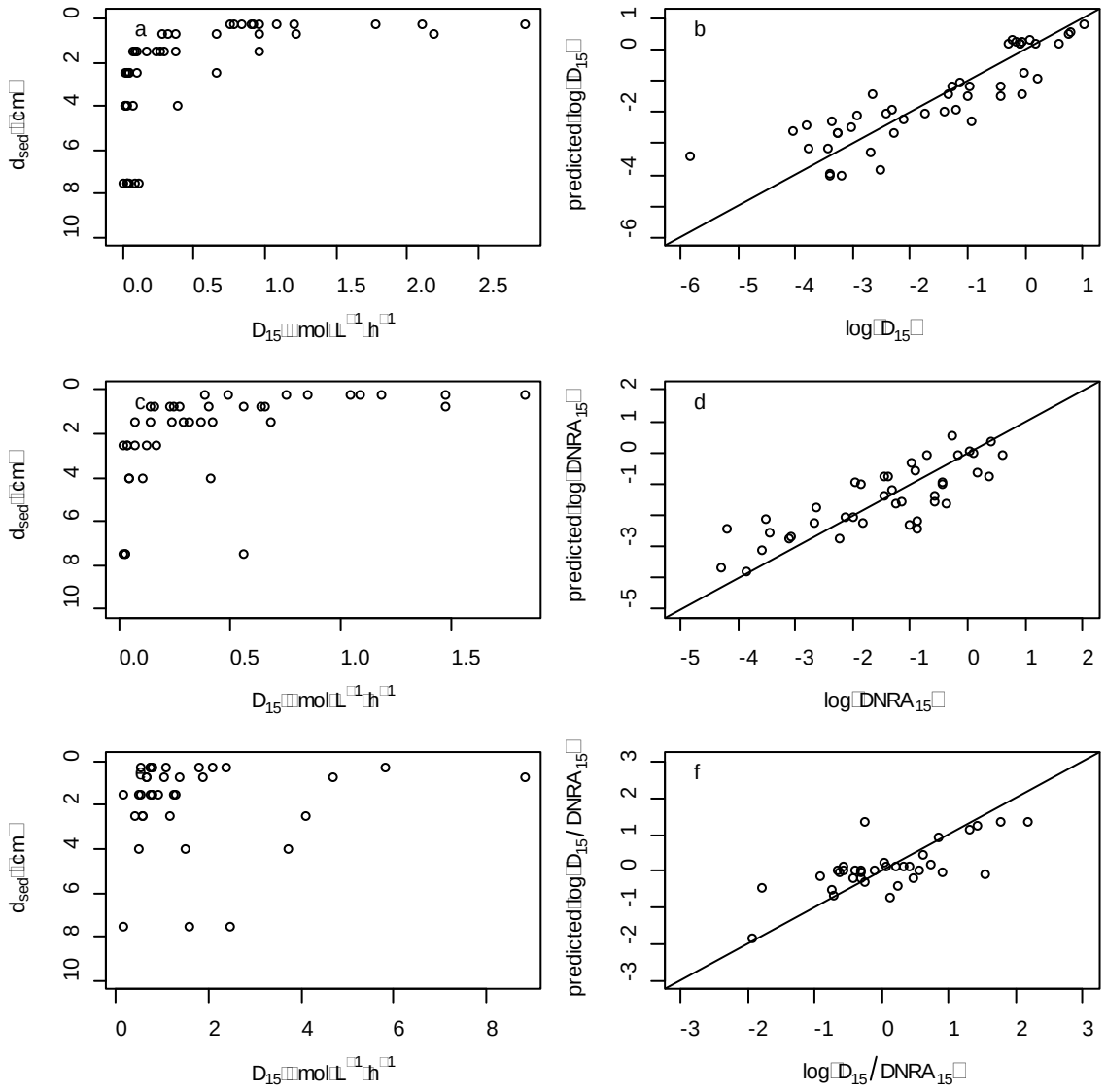

Figure S1: combined nitrogen fate data. (a) combined D_{15} data for all slices, as shown in Figure 2 (n = 46), showing exponential trend. (b) model fit for D_{15}, as described in Table 4. (c) combined $DNRA_{15}$ data for all slices, as shown in Figure 3 (n = 46), showing exponential trend. (d) model fit for $DNRA_{15}$, as described in Table 4. (e) combined $D_{15}/DNRA_{15}$ data for all slices, as shown in Figure 4 (n = 46), showing exponential trend. (f) model fit for $D_{15}/DNRA_{15}$, as described in Table 4.

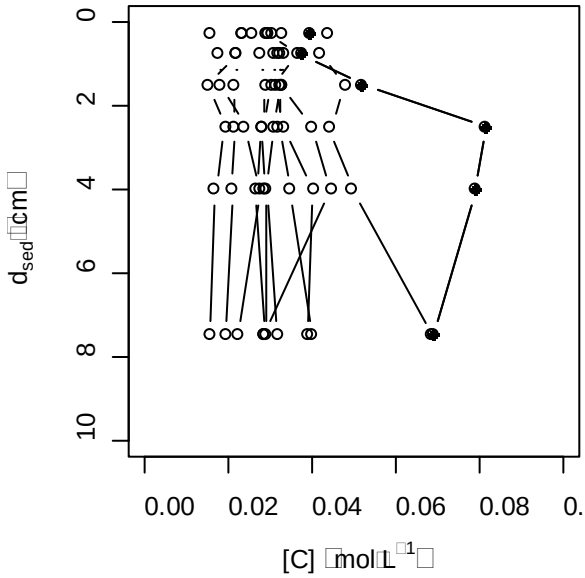

Figure S2: organic carbon concentration [C] profiles for all 11 sites. Filled markers are site MAL, all other sites are unfilled.

Table S1: Site water properties. Shown are depth (d in m), temperature (T, °C), chlorophyll-*a* (chl-*a* µg L^{-1}), dissolved oxygen saturation (DO, % air saturation) and salinity (Sal).

		Surface				Bottom			
	d_{OW}	T	chl-*a*	DO	Sal	T	chl-*a*	DO	Sal
HOP	4.0	10.0	3.0	102.5	2.8	13.1	3.2	79.7	30.3
CUR	3.2	10.0	2.7	76.0	1.3	11.8	1.5	91.4	29.9
AIR	1.5	10.5	0.0	83.7	0.0	10.4	3.0	82.9	1.5
WER	3.3	10.0	0.0	69.0	26.1	11.3	0.0	63.3	33.9
YAR	4.3	9.0	0.0	80.6	2.8	11.7	0.0	37.9	31.5
PAT	2.9	10.2	1.5	100.9	19.5	10.6	0.0	99.4	36.4
LW	3.0	8.1	0.0	87.2	13.7	8.3	1.3	86.8	14.1
LKN	8.0	9.6	1.3	83.8	27.6	12.9	0.0	20.2	32.3
TAM	5.5	11.9	0.0	88.1	9.6	10.9	4.2	76.6	13.6
WIN	5.5	12.8	0.0	96.1	32.0	13.9	1.9	80.9	35.0
MAL	6.2	11.3	5.7	86.8	26.5	13.6	2.5	5.6	33.8

Table S2: nutrient concentrations in bottom waters (µmol L^{-1}) and pore waters (shown as mmol m^{-2} integrated over depth) of each estuary.

	Bottom water			Pore water			
	$[NO_x]_{OW}$	$[NH_4^+]_{OW}$	$[FRP]_{OW}$	$[NH_4^+]$	[FRP]	$[Fe^{2+}]$	$[Fe^{asc}]$
HOP	6.7	128	14.5	140	19	0.14	66
CUR	49	121	0.85	320	12	19	170
AIR	17	6.1	0.35	8.6	2.3	0.36	43
WER	30	85	8.0	68	11	0.20	340
YAR	7.3	129	3.9	87	15	1.0	170
PAT	3.4	2.1	2.1	8.4	1.6	2.5	660
LW	26	6.4	0.33	26	3.1	4.5	88
LKN	36	22	0.23	24	3.3	1.4	24
TAM	0.53	6.6	0.29	8.7	1.0	4.6	330
WIN	3.2	7.4	0.33	24	1.5	7.1	290
MAL	0.50	67	1.0	150	9.2	0.26	92

Table S3: Faunal counts per 4 cores. Abundance in unit m^{-2} can be calculated by multiplying by 73. Note that there were no fauna found at HOP.

Phylum	Class	Order	Family	Genus	Species	TAM	MAL	WIN	YAR	WER	AIR	CUR	LW	LKN	PAT
Annelida			Spionidae	carazziella	sp	24								12	2
				prionospio	cirrifera	1									
				polydora	sp					13					
				unid. spionid	spp?	115	8	41	12	58	7	88	1	9	
				unid. spionid	sp										5
				magelona	sp										1
			Nephtyidae	Nephtys	sp	1					5	1			
			Orbiniidae	Scoloplos	normalis	6									
			Opheliidae	Armandia	sp			9							
			Maldanidae	Unidentified maldanid	sp			1							
			Sabellidae	Unidentified sabellid	spp	6	6			1					
			Oweniidae	Owenia	fusiformis	4									
			Nereididae	Australonereis	ehlersi	1				1	2		3		
				Simplisetia	sp.								1		
				Unidentified nereid	sp1			1							
				Unidentified nereid	sp2					1					
				Unidentified nereid	sp3									2	
				Unidentified nereid	sp4										1
			Capitellidae	unid. capitellid	spp.				1	31			121	1	
				unid. capitellid	sp1										5
				unid. capitellid	sp2										39
			Cirratulidae	unid. cirratulid										6	10
			Lumbrineridae	lumbrinereis	latreilli										4
			unid. polychaete		sp1									1	
			unid. polychaete		sp2									1	

Phylum	Class	Order	Family	Genus	Species	TAM	MAL	WIN	YAR	WER	AIR	CUR	LW	LKN	PAT
Nemertea				unid. nemertea	sp.	10									
Platyhelminthes				unid. platyhelminthes		1									
Mollusca			Haminoeidae	unid. (liloa brevis?)		34									
	Gastropoda		Nassariidae	Tritia	burchardi	2				1					1
				unid.	spp						1				
				Tatea	rufilabris							1			
	Bivalvia		Tellinidae	Macomona	deltoidalis	5								14	1
			Mytilidae	Arcuatula	senhousia	1								10	
		Amphipoda				17		1		2	2				
		Cumacea				2		2				12			
		Copepoda						3	1						
Chordata	Ascidiacea													2	
	Insecta		Chironomidae									1		1	

	TAM	MAL	WIN	YAR	WER	AIR	CUR	LW	LKN	PAT
Total annelids	169	14	52	13	105	14	89	126	32	67
Annelid Richness	10	2	4	2	6	3	2	4	7	8
Total fauna	230	14	58	14	108	17	103	126	59	69
Fauna Richness	16	2	7	3	8	5	5	4	11	10

Table S4: full data set used for regression. NA indicates rates were not significant (see text). For explanation of symbols and units, see Table 3.

site	d_{sed}	D_{15}	$DNRA_{15}$	$D_{15}/DNRA_{15}$	$[Fe^{2+}]$	$[Fe^{asc}]$	$[NH_4^+]$	[AVS]	[C]	$[NO_x]_{OW}$	fert	DO_{OW}	T_{OW}	F	$[chl\text{-}a]_{OW}$	$[NH_4^+]_{OW}$
HOP	0.25	2.10	1.19	1.77	4	8711	464	34382	0.015	6.7	88.7	6.87	13.1	0	3.20	127.6
HOP	0.75	NA	NA	NA	1	11217	698	46842	0.018	6.7	88.7	6.87	13.1	0	3.20	127.6
HOP	1.5	0.07	0.42	0.17	1	7509	960	64868	0.018	6.7	88.7	6.87	13.1	0	3.20	127.6
HOP	2.5	NA	0.02	NA	2	7725	1013	106847	0.024	6.7	88.7	6.87	13.1	0	3.20	127.6
HOP	4	0.02	0.04	0.49	1	5493	1211	88472	0.027	6.7	88.7	6.87	13.1	0	3.20	127.6
HOP	7.5	NA	NA	NA	1	3089	1950	48494	0.022	6.7	88.7	6.87	13.1	0	3.20	127.6
CUR	0.25	0.84	1.09	0.77	143	26419	438	8931	0.031	48.8	86.6	8.14	11.8	103	1.50	121.2
CUR	0.75	1.22	0.65	1.87	278	25337	771	25150	0.033	48.8	86.6	8.14	11.8	103	1.50	121.2
CUR	1.5	0.26	0.29	0.89	308	22196	1087	60158	0.033	48.8	86.6	8.14	11.8	103	1.50	121.2
CUR	2.5	0.03	0.03	1.15	237	21872	2171	38801	0.031	48.8	86.6	8.14	11.8	103	1.50	121.2
CUR	4	NA	NA	NA	118	12989	3260	54013	0.029	48.8	86.6	8.14	11.8	103	1.50	121.2
CUR	7.5	NA	0.03	NA	186	8025	4228	71141	0.032	48.8	86.6	8.14	11.8	103	1.50	121.2
AIR	0.25	1.78	0.75	2.37	4	6065	29	0	0.044	17.2	14	9.11	10.4	17	3.00	6.1
AIR	0.75	NA	0.40	NA	3	4470	29	0	0.042	17.2	14	9.11	10.4	17	3.00	6.1
AIR	1.5	NA	NA	NA	3	1740	48	37	0.048	17.2	14	9.11	10.4	17	3.00	6.1
AIR	2.5	NA	NA	NA	2	1944	47	0	0.044	17.2	14	9.11	10.4	17	3.00	6.1
AIR	4	NA	NA	NA	2	910	74	0	0.050	17.2	14	9.11	10.4	17	3.00	6.1
AIR	7.5	NA	NA	NA	5	1136	117	0	0.069	17.2	14	9.11	10.4	17	3.00	6.1
WER	0.25	2.83	0.49	5.83	9	20078	154	63208	0.029	29.9	56.4	5.64	11.3	108	0.00	85.4
WER	0.75	2.19	0.25	8.84	5	12974	155	177217	0.037	29.9	56.4	5.64	11.3	108	0.00	85.4
WER	1.5	0.96	NA	NA	3	9063	232	61017	0.030	29.9	56.4	5.64	11.3	108	0.00	85.4
WER	2.5	0.66	0.16	4.12	2	8709	289	118154	0.028	29.9	56.4	5.64	11.3	108	0.00	85.4
WER	4	0.39	0.11	3.71	1	9494	411	96649	0.027	29.9	56.4	5.64	11.3	108	0.00	85.4
WER	7.5	0.12	NA	NA	1	14713	1061	182740	0.029	29.9	56.4	5.64	11.3	108	0.00	85.4
YAR	0.25	0.95	1.83	0.52	50	22208	312	10386	0.030	7.3	43.6	3.4	11.7	14	0.00	128.7
YAR	0.75	NA	0.15	NA	37	22288	414	7031	0.031	7.3	43.6	3.4	11.7	14	0.00	128.7
YAR	1.5	0.37	0.68	0.54	27	9646	446	57189	0.031	7.3	43.6	3.4	11.7	14	0.00	128.7

YAR	2.5	0.05	0.12	0.41	15	8529	649	18138	0.033	7.3	43.6	3.4	11.7	14	0.00	128.7
YAR	4	NA	NA	NA	4	4531	873	105186	0.040	7.3	43.6	3.4	11.7	14	0.00	128.7
YAR	7.5	0.04	NA	NA	3	6451	1098	136531	0.039	7.3	43.6	3.4	11.7	14	0.00	128.7
PAT	0.25	0.91	NA	NA	10	42101	51	0	0.026	3.4	57.1	8.71	10.6	69	0.00	2.1
PAT	0.75	0.28	0.27	1.05	20	39494	49	0	0.027	3.4	57.1	8.71	10.6	69	0.00	2.1
PAT	1.5	0.09	0.07	1.25	33	36717	54	0	0.029	3.4	57.1	8.71	10.6	69	0.00	2.1
PAT	2.5	0.04	0.07	0.56	35	22699	69	0	0.028	3.4	57.1	8.71	10.6	69	0.00	2.1
PAT	4	0.07	0.05	1.50	32	16735	94	313	0.029	3.4	57.1	8.71	10.6	69	0.00	2.1
PAT	7.5	NA	NA	NA	21	19949	96	1381	0.029	3.4	57.1	8.71	10.6	69	0.00	2.1
LW	0.25	1.21	NA	NA	49	13391	55	0	0.023	0.4	33	9.8	8.3	126	1.30	9.5
LW	0.75	0.38	0.56	0.68	26	8185	84	7	0.022	0.4	33	9.8	8.3	126	1.30	9.5
LW	1.5	0.17	0.37	0.47	150	4798	125	321	0.015	0.4	33	9.8	8.3	126	1.30	9.5
LW	2.5	NA	NA	NA	106	6113	167	13925	0.019	0.4	33	9.8	8.3	126	1.30	9.5
LW	4	NA	NA	NA	48	4334	224	11258	0.017	0.4	33	9.8	8.3	126	1.30	9.5
LW	7.5	0.03	0.02	1.59	12	3890	362	8703	0.015	0.4	33	9.8	8.3	126	1.30	9.5
LKN	0.25	0.79	0.38	2.07	8	7038	62	11200	0.023	1.9	14.7	2.02	12.9	59	0.00	45.9
LKN	0.75	0.32	0.23	1.39	11	4394	80	12564	0.022	1.9	14.7	2.02	12.9	59	0.00	45.9
LKN	1.5	0.10	0.14	0.73	27	3042	134	10925	0.022	1.9	14.7	2.02	12.9	59	0.00	45.9
LKN	2.5	0.02	0.03	0.56	20	2890	183	7991	0.021	1.9	14.7	2.02	12.9	59	0.00	45.9
LKN	4	0.02	NA	NA	14	1390	234	10170	0.021	1.9	14.7	2.02	12.9	59	0.00	45.9
LKN	7.5	0.03	0.01	2.48	10	861	303	3018	0.019	1.9	14.7	2.02	12.9	59	0.00	45.9
TAM	0.25	0.76	1.04	0.73	90	29065	34	1826	0.033	0.5	1.9	7.71	10.9	230	4.20	6.6
TAM	0.75	NA	0.64	NA	27	25644	46	1571	0.032	0.5	1.9	7.71	10.9	230	4.20	6.6
TAM	1.5	0.24	0.31	0.77	111	17251	58	5532	0.033	0.5	1.9	7.71	10.9	230	4.20	6.6
TAM	2.5	0.10	NA	NA	55	26469	68	5310	0.040	0.5	1.9	7.71	10.9	230	4.20	6.6
TAM	4	0.03	NA	NA	58	14315	71	14156	0.045	0.5	1.9	7.71	10.9	230	4.20	6.6
TAM	7.5	0.04	NA	NA	23	14254	112	4899	0.029	0.5	1.9	7.71	10.9	230	4.20	6.6
WIN	0.25	0.91	0.85	1.07	41	37756	45	0	0.030	3.2	0.5	6.67	13.9	58	1.90	7.4
WIN	0.75	0.66	0.14	4.69	78	32610	76	462	0.032	3.2	0.5	6.67	13.9	58	1.90	7.4
WIN	1.5	NA	NA	NA	146	36077	122	5533	0.033	3.2	0.5	6.67	13.9	58	1.90	7.4

WIN	2.5	NA	NA	NA	129	24762	153	12523	0.032	3.2	0.5	6.67	13.9	58	1.90	7.4
WIN	4	NA	0.41	NA	95	19531	212	29853	0.035	3.2	0.5	6.67	13.9	58	1.90	7.4
WIN	7.5	0.00	NA	NA	38	18789	323	61805	0.040	3.2	0.5	6.67	13.9	58	1.90	7.4
MAL	0.25	1.08	1.47	0.73	11	6815	213	15157	0.039	0.5	2.9	0.47	13.6	14	2.50	66.9
MAL	0.75	0.97	1.47	0.66	10	4841	391	44838	0.038	0.5	2.9	0.47	13.6	14	2.50	66.9
MAL	1.5	0.30	0.24	1.27	9	8445	592	13715	0.052	0.5	2.9	0.47	13.6	14	2.50	66.9
MAL	2.5	0.05	NA	NA	1	4142	862	57767	0.082	0.5	2.9	0.47	13.6	14	2.50	66.9
MAL	4	NA	NA	NA	1	2966	1203	12257	0.079	0.5	2.9	0.47	13.6	14	2.50	66.9
MAL	7.5	0.08	0.56	0.15	1	2794	2147	18161	0.069	0.5	2.9	0.47	13.6	14	2.50	66.9

Table S5: Integrated data displayed in Figure 6. For explanation of symbols and units, see text.

site	D_{14}	$DNRA_{14}$	$D_{14}/DNRA_{14}$	$[Fe^{2+}]$	[AVS]	[C]	$[NO_x]_{ow}$
HOP	1.90	5.75	0.33	39.77	1054.80	0.35	6.68
CUR	36.07	29.19	1.24	5184.87	771.99	0.65	48.79
AIR	14.64	3.97	3.69	60.94	0.37	0.91	17.23
WER	152.83	18.95	8.06	99.62	1812.30	0.63	29.86
YAR	9.93	13.42	0.74	708.25	658.98	0.61	7.33
PAT	2.56	1.80	1.42	483.88	0.00	0.55	3.39
LW	3.45	3.42	1.01	1872.30	3.25	0.38	0.43
LKN	5.41	0.65	8.37	368.76	228.07	0.44	1.88
TAM	2.74	2.69	1.02	1699.00	72.31	0.65	0.53
WIN	6.31	4.42	1.43	2049.79	57.64	0.64	3.21
MAL	5.17	7.65	0.68	194.94	437.13	0.91	0.50